Supporting Information

Assessing optical and electrical properties of highly active IrO_x catalysts for the electrochemical oxygen evolution reaction via spectroscopic ellipsometry

René Sachse[a,d], Mika Pflüger[b], Juan-Jesús Velasco-Vélez[c], Mario Sahre[a], Jörg Radnik[a], Michael Bernicke[d], Denis Bernsmeier[d], Vasile-Dan Hodoroaba[a], Michael Krumrey[b], Peter Strasser[d], Ralph Kraehnert* [d] and Andreas Hertwig* [a]

[a] Federal Institute for Materials Research and Testing (BAM), Unter den Eichen 44-46, 12203 Berlin, Germany
[b] Physikalisch-Technische Bundesanstalt (PTB), Abbestraße 2-12, 10587 Berlin, Germany
[c] Fritz-Haber-Institut der Max-Planck-Gesellschaft, Faradayweg 4-6, 14195 Berlin, Germany.
[d] Technische Universität Berlin, Faculty II Mathematics and Natural Sciences, Institute of Chemistry, Straße des 17. Juni 135, 10623 Berlin, Germany.

Corresponding Authors: *ralph.kraehnert@tu-berlin.de; *andreas.hertwig@bam.de

SI 1. (HR)-SEM images in top-view and cross-section mode of mesoporous IrO_x films

SEM images of mesoporous iridium oxide film deposited on silicon substrates, calcined at temperatures between 300 and 600 °C. The first row shows the SEM images in top-view mode of each film. The Fast-Fourier Transformation (FFT) insets indicates the ordered structure of the mesopores with different orientations. High-resolution (HR) images (second row) show pore openings of about 14 to 16 nm. SEM images in cross-section (third row) present the film thickness of each film.

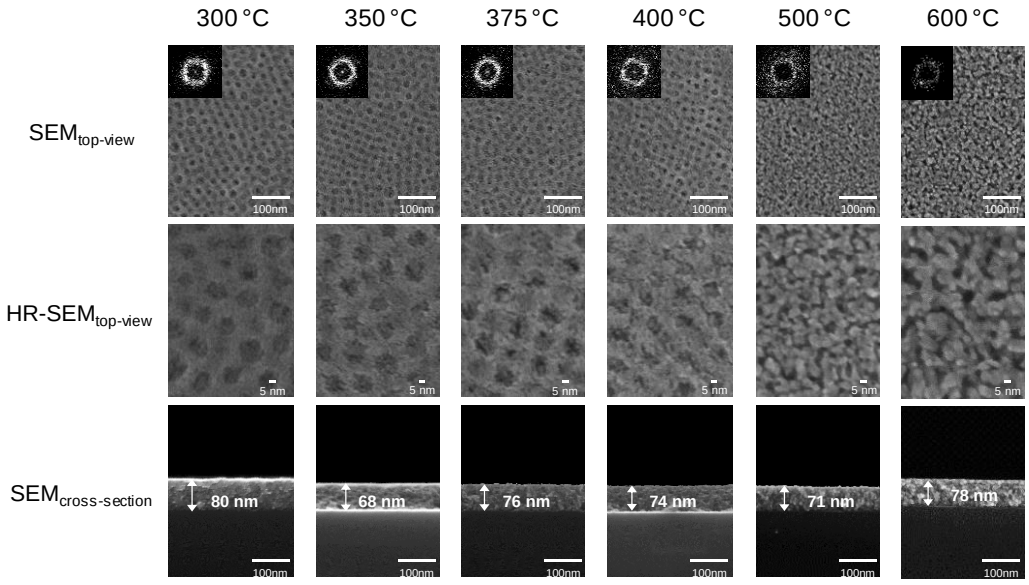

Figure S1: SEM images of deposited mesoporous iridium oxide films on silicon substrates. The first row shows SEM images in top-view mode of the films calcined at the given temperature. The second row displays high resolution images of the film and the third row presents cross-section images with layer thicknesses of the films.

SI 2. X-Ray reflectometry fitting

In XRR, the specular reflectivity of a layered sample is measured at a range of glancing incidence angles. The X-rays are reflected by interfaces at different depth and interfere constructively or destructively depending on the relative optical path, leading to minima and maxima in the specular reflectivity. For simple samples, thicknesses can be calculated directly from the frequency of the reflectivity oscillations,[1] but for the determination of densities and for more complex samples, fitting of the measured reflectivity curve to a physical model is necessary

To determine the film thickness and density from the XRR measurements, the reflectivity $R(\Theta)$ of each sample was modelled using the matrix method.[2] For the simulation, we model the sample as a Si substrate with three layers on top: a layer of natural oxide consisting of SiO_2, the mesoporous IrO_2 layer, and a carbonaceous contamination layer on top. The thicknesses t of all three layers are left as a variable parameter. For the X-ray refractive index and the density of the Si and SiO_2 layers, tabulated values were used.[3] The density of the mesoporous IrO_2 layer ρ_{IrO_2} and the carbonaceous contamination layer ρ_C are left as variable parameters, and the respective refractive indices were calculated from the density using tabulated bulk densities and refractive indices. At each interface between layers, a debye-waller-like factor was introduced to account for roughness and interdiffusion, giving four additional variable parameters $\sigma_{1..4}$. In order to model the measured XRR signal from the simulated reflectivity, additional effects of the measurement have to be simulated. For the measurements conducted with the Cu Kα lab instrument, the incident X-ray intensity is not known from the measurements and is therefore treated as a variable parameter f. For the beamline measurements at lower photon energies that were conducted without a monitoring diode, the incident beam intensity was measured directly before and after the XRR measurement. In this case, the uncertainty of the incident X-ray intensity was estimated conservatively to be 10%, and f is treated as a variable parameter within this uncertainty. For the lab instrument measurements as well as the beamline measurements at lower photon energies, the dark current of the photo diode is not well known and is treated as a variable parameter I_{dark}. To account for a possible misalignment of the sample with regard to the incident beam, the offset of the incidence angle Θ_0 was treated as a variable parameter. To simulate the effects of divergence in the incident beam, the simulated reflectivity is convolved with the Gaussian beam profile, the width of the Gaussian σ_Θ is considered a variable parameter. Finally, at very small incidence angles the footprint of the beam is longer than the sample, leading to a smaller effective incident intensity. For this, the length of the sample relative to the height of the X-ray beam h is treated as a variable parameter. In total, there are 12 to 14 variable parameters in our model, but some of them with tight limits from separate measurements. The model formula then reads

$$I_s(\Theta) = R\left(t_{SiO_2}, t_{IrO_2}, t_C, \rho_{IrO_2}, \rho_C \sigma_1, \sigma_2, \sigma_3, \sigma_4; \Theta + \Theta_0\right) * g(\sigma_\Theta; \Theta) \;\; f\, erf\left(sin(\Theta + \Theta_0)\, h/\sqrt{2}\right) + I_{dark} \quad (1)$$

with the error function erf.

To obtain uncertainties for the reconstructed parameters, the affine invariant Markov chain Monte Carlo (MCMC) algorithm[4] as implemented in the emcee software package[5] was used. For the MCMC evaluation, we use the likelihood function

$$\mathcal{L} = \prod_{\Theta} \frac{1}{\sqrt{2\pi u(\Theta)^2}} \exp\left(\frac{-\left(I_s(\Theta) - I_m(\Theta)\right)^2}{2u(\Theta)^2}\right) \quad (2)$$

with the simulated intensity $I_s(\Theta)$, the measured intensity $I_m(\Theta)$ and the uncertainty $u(\Theta)$. The uncertainty is estimated using the error model

$$u(\Theta) = aI_s(\Theta) + b \quad (3)$$

with the uncertainty factors *a* and *b*. For the beamline measurement at 8048 eV, *b* is estimated from the standard deviation of a dark current measurement, and *a* is treated as a variable parameter. For all other measurements, *a* and *b* are treated as a variable parameter.

For the MCMC evaluation, gaussian priors with large widths are assumed for all parameters that are not *a priori* constrained by other measurements, and starting positions for the algorithm are randomly drawn from the prior. The evaluation was done separately for each sample. Depending on convergence behavior, the first about 15 million function evaluations were discarded as burn-in, and the chain was run for at least 24 million additional function evaluations. Final parameter values and uncertainties were obtained from the 66% confidence interval of the MCMC result.

To compare the accuracy of the used XRR model, a sample (375 °C) was measured at a four-crystal monochromator beamline and additionally with cross-sectional SEM, ellipsometry and ellipsometric porosimetry (Figure S2). Both the layer thickness and porosity values correspond well between the techniques used.

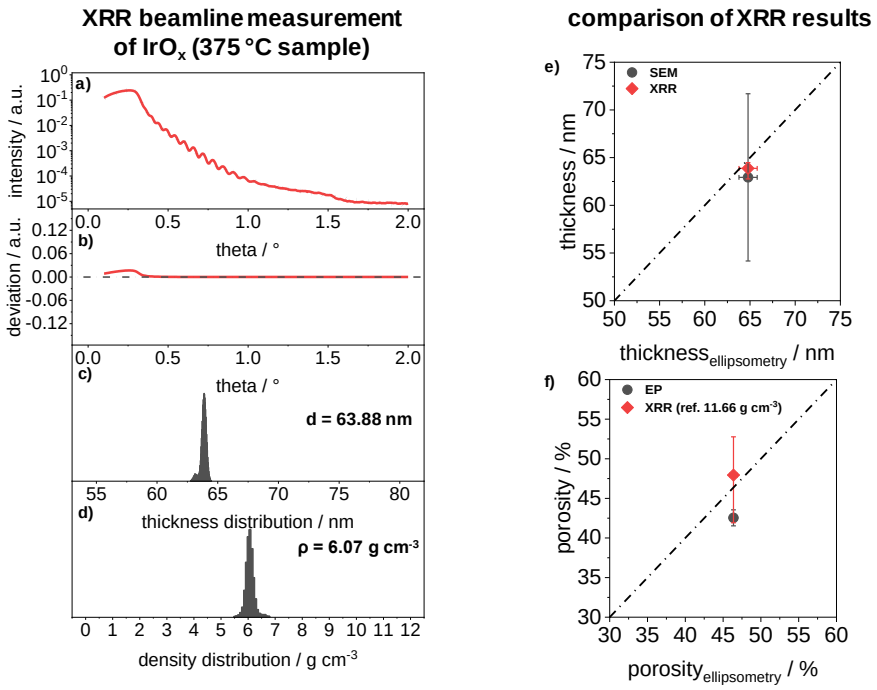

Figure S2: Validation of the XRR modeling of an IrO_x sample calcined at 375 °C, measured at a four-crystal monochromator beamline. a) and b) show the XRR measurement with fit results. c) derived film thickness and d) film porosity. e) comparison of film thickness by SEM, XRR and SE. f) comparison of porosity by XRR, SE and EP.

Figure S3 displays the XRR measurements of the lab instrument with their fit results of the IrO_x calcination series. The sample calcined at 300 °C shows no interference in the XRR measurement, which leads to the very high deviation in the film thickness and a higher deviation in the density. The difference in thickness and density of the 375 °C sample is due to the use of two samples. The beamline sample was used to develop the XRR model, which was then applied to the samples of the calcination series.

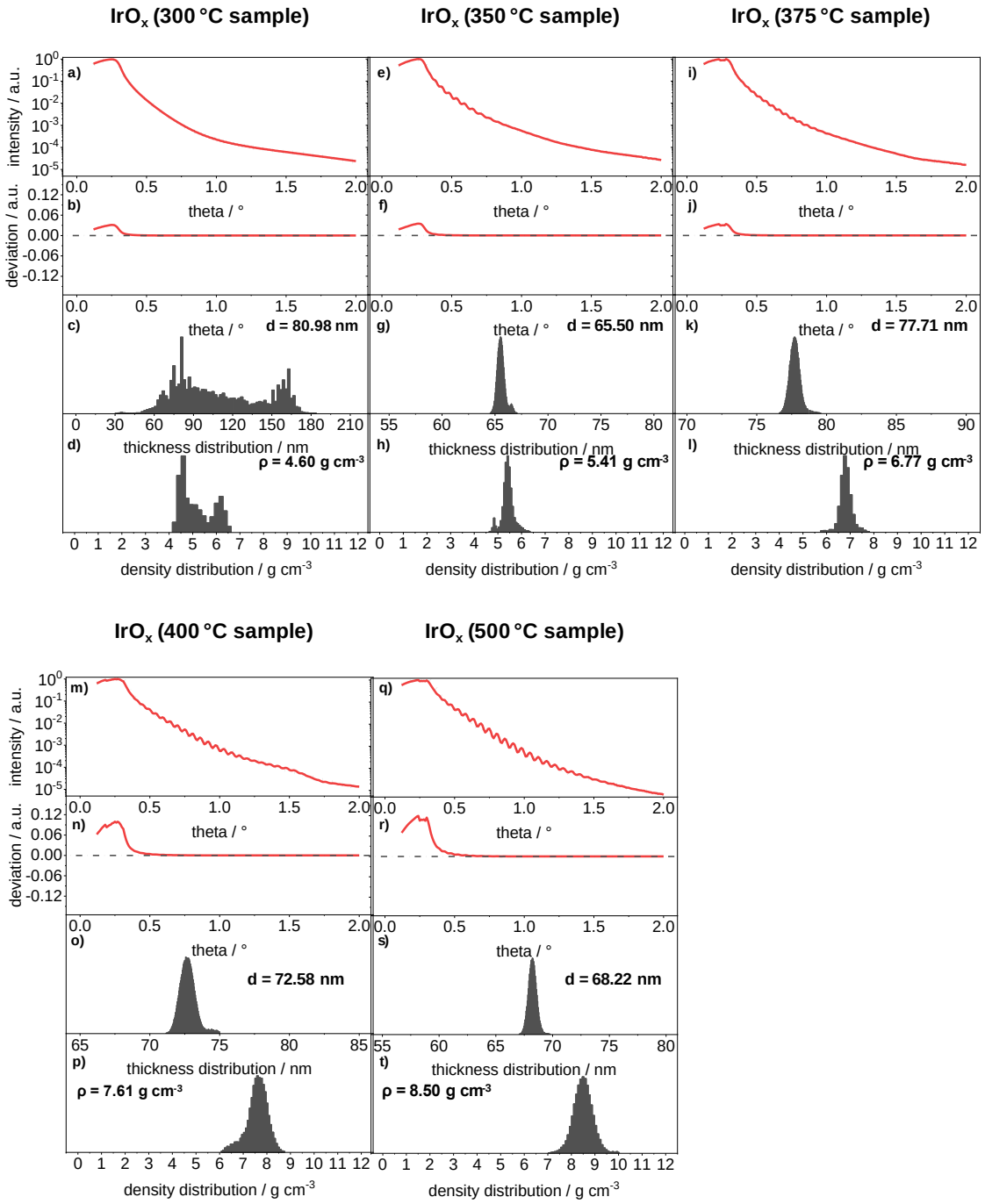

Figure S3: XRR data with fits and the obtained thickness and density distribution of measured mesoporous iridium oxide films on silicon substrates. a), e), i), m) and q) show the measured data and the fit of each mesoporous film. b), f), j), n) and r) indicate the deviations of the XRR fits. c), g), k), o) and s) present the film thickness distributions and d), h), l), p) and t) the density distributions of each film.

SI 3. X-ray diffraction measurements of mesoporous iridium oxide films

X-ray diffractograms of mesoporous iridium oxide films with indication of the reflections of cubic (ccp) iridium (PDF: 00-006-0598) and rutile iridium oxide (PDF: 00-015-0870). Films calcined between 300 and 375 °C show a low crystalline structure, which is indicated by a broad reflection around 34.6°. These reflections can attribute to (101) plane of rutile IrO_2. At 400 °C the iridium oxide film becomes more crystalline due to an additionally reflection at 28°, which can attribute to the (110) plane. The film calcined at 500 °C and 600 °C show several reflections, which can attribute to the rutile phase of iridium oxide. In all cases, no indication of a cubic iridium phase is observed.

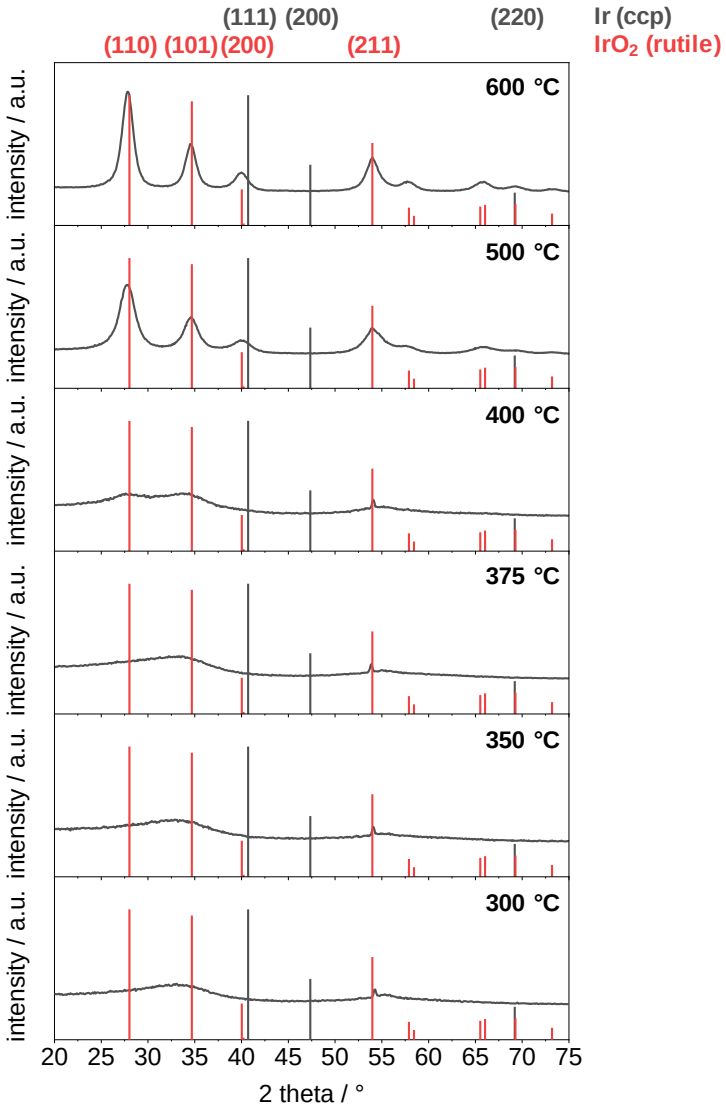

Figure S4: X-ray diffractograms of mesoporous iridium oxide films deposited on silicon wafers, with reflection intensities of cubic (ccp) iridium (PDF: 00-006-0598) and rutile iridium oxide (PDF: 00-015-0870).

SI 4. Electrochemical analysis of mesoporous IrO_x films

Catalyst films were deposited on conductive titanium substrates and calcined in air for 5 minutes. 5 mm circular catalyst films were studied in the OER regime and in the lower potential range in N_2 purged 0.5M H_2SO_4. Fifty cyclic voltammograms (CV) recorded at potentials between 1.2 V_{RHE} and 1.65 V_{RHE} with a scan rate of 6 mV s^{-1}. Basic cyclic voltammetry measurements were recorded in a potential window of 0.4 V_{RHE} and 1.4 V_{RHE} with a scan rate of 50 mV s^{-1}. Before each cyclic voltammetry measurement, potential electrochemical impedance spectroscopy (PEIS) was recorded to correct ohmic losses (iR correction).

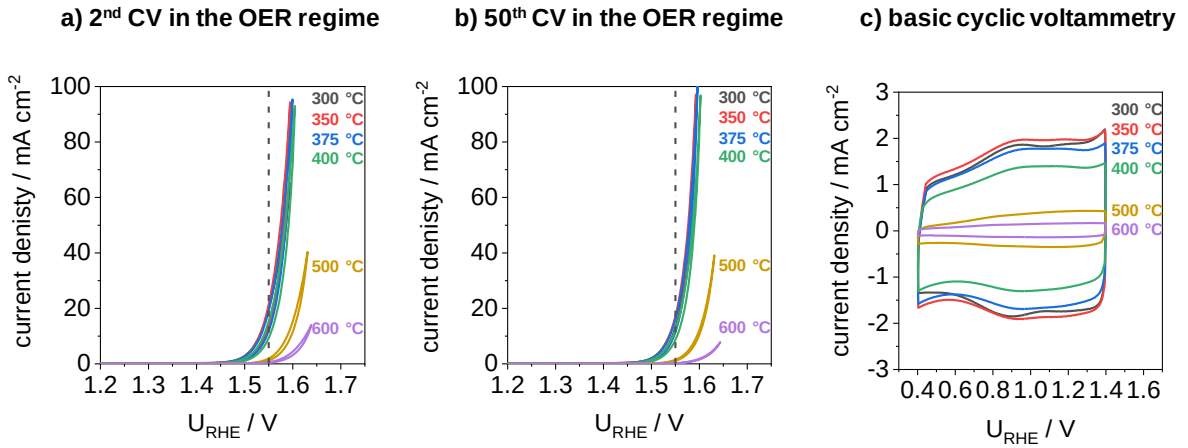

Figure S5: Electrochemical analysis of mesoporous iridium oxide catalyst films. Catalyst films were deposited on conductive titanium substrates and calcined for 5 min in air. Electrochemical studies in the OER regime and in the lower potential range were recorded in N_2 purged 0.5M H_2SO_4. a) 2nd cycle and b) 50th cycle in the OER regime with a cycle speed of 6 mV s^{-1}. c) basic cyclic voltammetry in a lower potential window with a cycle speed of 50 mV s^{-1}.

SI 5. Spectroscopic ellipsometry (SE) model evaluation

SE measures the change in the polarization state of light, that is reflected or transmitted from a sample surface. The change in the polarization of light, which is oriented in p- and s-directions relative to the plane of incident, is described by an amplitude ratio tan(Ψ) and a phase difference Δ. The resulting complex reflectance ratio ρ is expressed as:

$$\rho = \frac{r_p}{r_s} = \tan(\Psi) \cdot e^{i\Delta} \quad (4)$$

where r_p and r_s describe the complex Fresnel reflection coefficients for p- and s-polarized light, respectively. Ellipsometric measurements are usually used to determine optical constants and film thicknesses of transparent and semi-transparent films. Absorbent layers are more complicate to measure due to a strong correlation between film thickness and optical constants, which can prevent a unique solution, especially if the porosity is an additional unknown parameter. However, optical measurements have the advantage of non-destructive measurements and offer the possibility for in-situ applications in which film thickness and optical constants have to be determined quickly and precisely. For a unique solution for thickness, dielectric constants and porosity, an increase of measurement information or reduction of unknown sample properties is required. Various methods can be used to reduce the correlation of the unknown parameters of absorbing films, e.g. the analysis of multiple samples, measurements with different angles of incidence, or an improvement in interference.[6] The latter method comprises the addition of a transparent film below the absorbing layer. This layer should have a sufficient layer thickness to generate interference in the absorbing layer. In order to reduce the correlation between optical constants and unknown parameters (e.g. layer thickness and porosity), simultaneous measurements and analyzes of multiple angles of incidence are required.

For the analysis with interference enhancement of mesoporous iridium oxide films, Si-substrates with thermal SiO_2 layers are used (Figure S6). By measuring the films with multiple angles of incident, the Ψ and Δ spectra can be modeled with an a-BEMA:

$$\sum_{n=1}^{m} f_n \frac{\varepsilon_n - \varepsilon_{eff,j}}{\varepsilon_{eff,j} + L_j(\varepsilon_n - \varepsilon_{eff,j})} = 0 \quad (5)$$

with depolarization factors:

$$L_j = \frac{U_x U_y U_z}{2} \int_0^\infty \frac{\left(s + U_j^2\right)^{-1} ds}{\sqrt{(s+U_x^2)(s+U_y^2)(s+U_z^2)}} \quad (6)$$

$\varepsilon_{eff,j}$ describes the effective major dielectric function (j = a, b, c), m the constituents of a mixture, f_n the fractions and ε_n the bulk-like dielectric functions.[7] The real depolarization factors L_j only depend on the real shape parameters U_j of the ellipsoid and the two relationships (U_x/U_z) and (U_y/U_z) serve to precisely define the shape.[7]

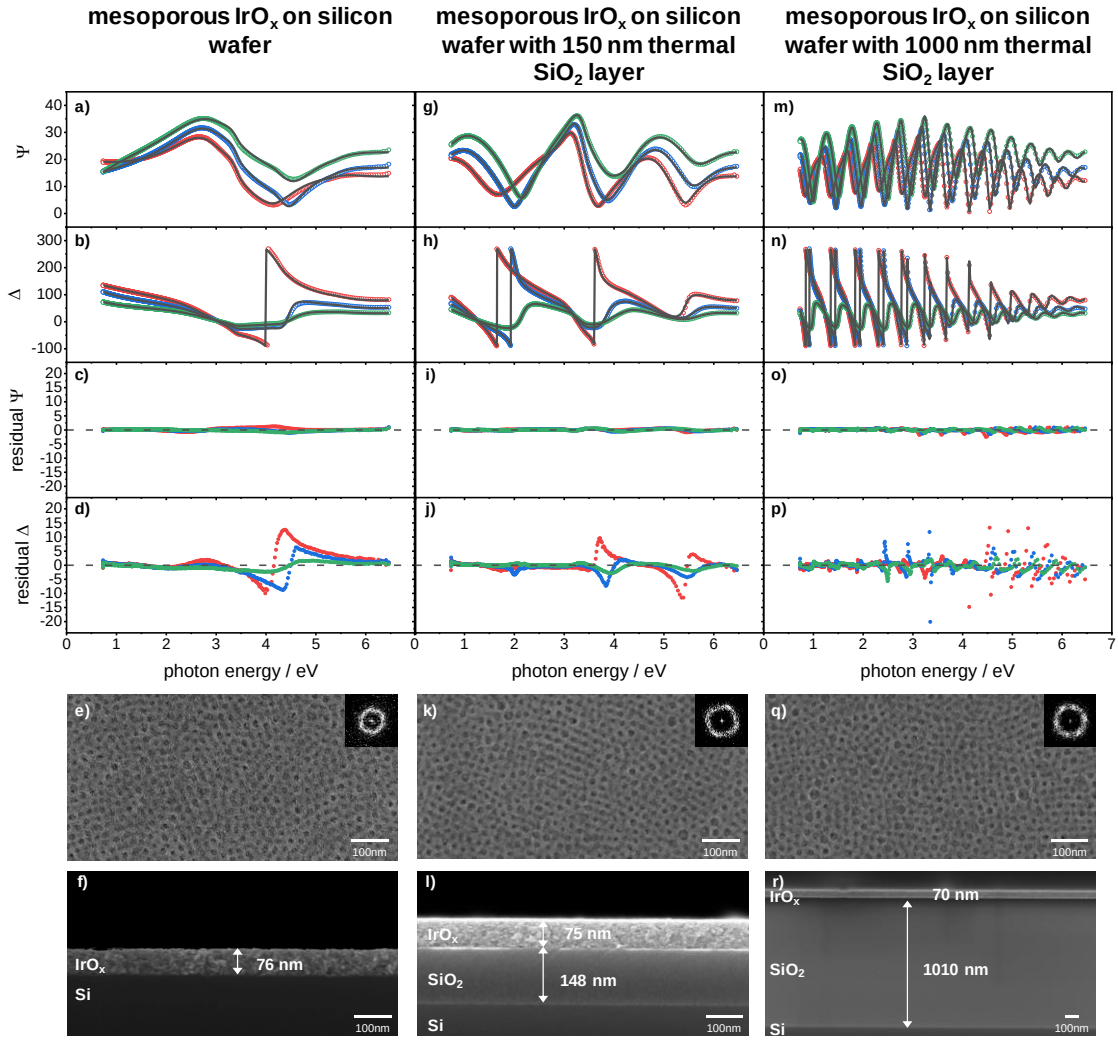

Figure S6: Data and fits as well as SEM images from the interference enhancement approach for spectroscopic ellipsometric measurements. a), g) and m) presents Psi spectra with fits for mesoporous iridium oxide films on a silicon wafer, a silicon wafer with a ~150 nm thermal SiO_2 layer and a silicon wafer with a ~1000 nm thermal SiO_2 layer, respectively. b), h, and n) show the corresponding Delta spectra. c), i), o) and d), j), p) reveal the residuals from the fits for the Psi and Delta spectra's, respectively. e), f), k), l), q) and r) show the SEM images of the films.

For the modelling of the dielectric function, a combination of a Drude type and three Lorentz type absorption bands are used. The Drude model is applicable to free-electron effects.[8, 9] _ENREF_34 The Drude model can be described with the resistivity ρ_R and the mean scattering time τ and is expressed by the following equation:

$$\varepsilon_{Drude}(E) = \frac{-\hbar^2}{\varepsilon_0 \, \rho_R \, (\tau \, E^2 + i \, \hbar \, E)} \tag{7}$$

with

$$\rho_R = \frac{m^*}{N \, q^2 \, \tau} = \frac{1}{q \, \mu \, N} \tag{8}$$

where E is the photon energy ($E = h\nu = \hbar\omega$), $\hbar$ the reduced Planck constant, ε_0 the vacuum dielectric constant, ρ_R the resistivity (Ohm cm), τ the mean scattering time (fs), m^* the electron effective mass ($9.11 \cdot 10^{-31}$ kg), N the electron concentration (cm^{-3}), q the electron charge ($1.60 \cdot 10^{-19}$ C) and μ the

electron mobility ($cm^2\ V^{-1}\ s^{-1}$).[10] Fit parameters for the Drude model are the resistivity ρ_R and the mean scattering time τ.

The Lorentz oscillator model is based on the classic theory of the interaction between light and matter and describes the bond between electrons and nucleus using a mass-spring system.[8, 9] The model can be used for frequency-dependent polarizations due to bound charge and can describe a direct interband transition. The Lorentz oscillator model is expressed as follows:

$$\varepsilon_{Lorentz}(E) = \frac{Amp_n\ Br_n\ En_n}{En_n^2 - E^2 - i\ E\ Br_n} \quad (9)$$

with Amp_n as the amplitude of the n^{th} oscillator (unitless), Br_n the full width at half-maximum of the n^{th} oscillator (eV) and En_n the center energy of n^{th} oscillator (eV).[11] The fit parameters of the Lorentz oscillators model are the amplitude Amp_n, the full width at half-maximum Br_n and the center energy En_n.

After modelling with interference enhancement, we fixed the center energy of each Lorentz oscillator. For the variation of the calcination temperature we used only the resistivity ρ_R and the mean scattering time τ of the Drude type as well as the amplitudes and full widths at half maximum of the three Lorentz oscillators as free parameters for the dielectric functions. Additionally, the real constant ε_∞ which is added to the ε_1 spectra served as well as free parameter for the dielectric functions. Thickness of the a-BEMA as well as the fraction of pores and the anisotropic geometry factor used as free parameters for the layer properties.

SI 6. Change of dielectric functions with calcination temperature

Change of the derived dielectric functions of mesoporous iridium oxide films calcined at temperatures between 300 and 600 °C from SE modelling.

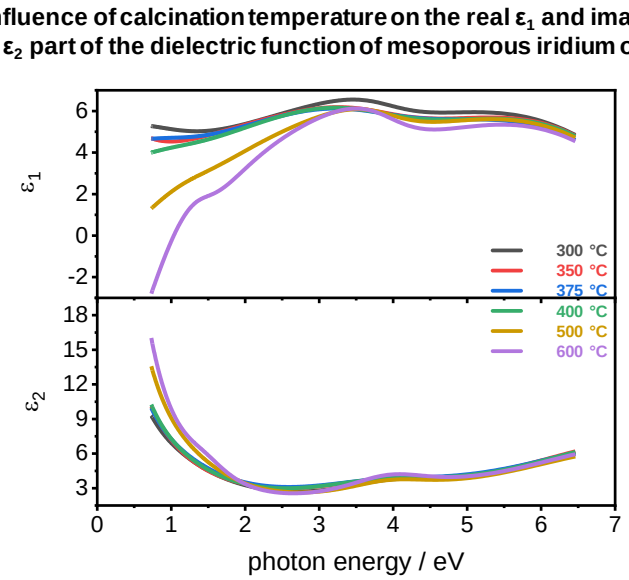

Figure S7: Real and imaginary part of the dielectric function of the iridium oxide material without void filling in dependence of the calcination temperature.

SI 7. Mean scattering time as a function of the calcination temperature of mesoporous IrO_x films

Mean scattering time τ from the fit parameter of the Drude model as a function of the calcination temperature.

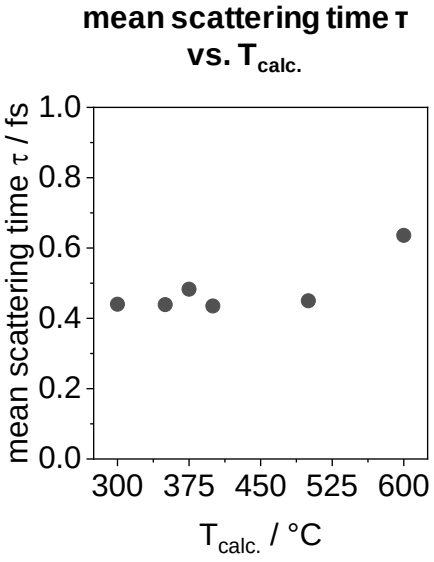

Figure S8: Mean scattering time τ of mesoporous iridium oxide films as a function of the calcination temperature.

SI 8. Thickness and porosity mapping via spectroscopic ellipsometry of a mesoporous IrO_x film calcined at 375 °C

SE mapping of a mesoporous IrO_x film on a Si wafer calcined at 375 °C provides information about the homogeneity of the derived thickness and porosity using the model described in SI 5. Figure S9a shows the layer thickness depending on the sample position. The black circles indicate the measured points and the lines the layer thickness profiles in the horizontal (Figure S9b) and vertical (Figure S9c) direction. In general, a homogeneous layer thickness is derived from the model for the complete sample. The layer thickness profiles in the horizontal direction show slightly lower values of the layer thickness at the edges, while in the vertical direction a strong increase is obtained from the substrate surface to the deposited layer, which then decrease slightly towards the top of the layer. However, changes in film thickness are less than 5 nm, considering the deviation. A similar behavior is also observed for the porosity of the IrO_x film (Figure S9d), where the derived values indicate the same porosity in the horizontal (Figure S9e) and vertical (Figure S9f) line profile (except for the Si substrate).

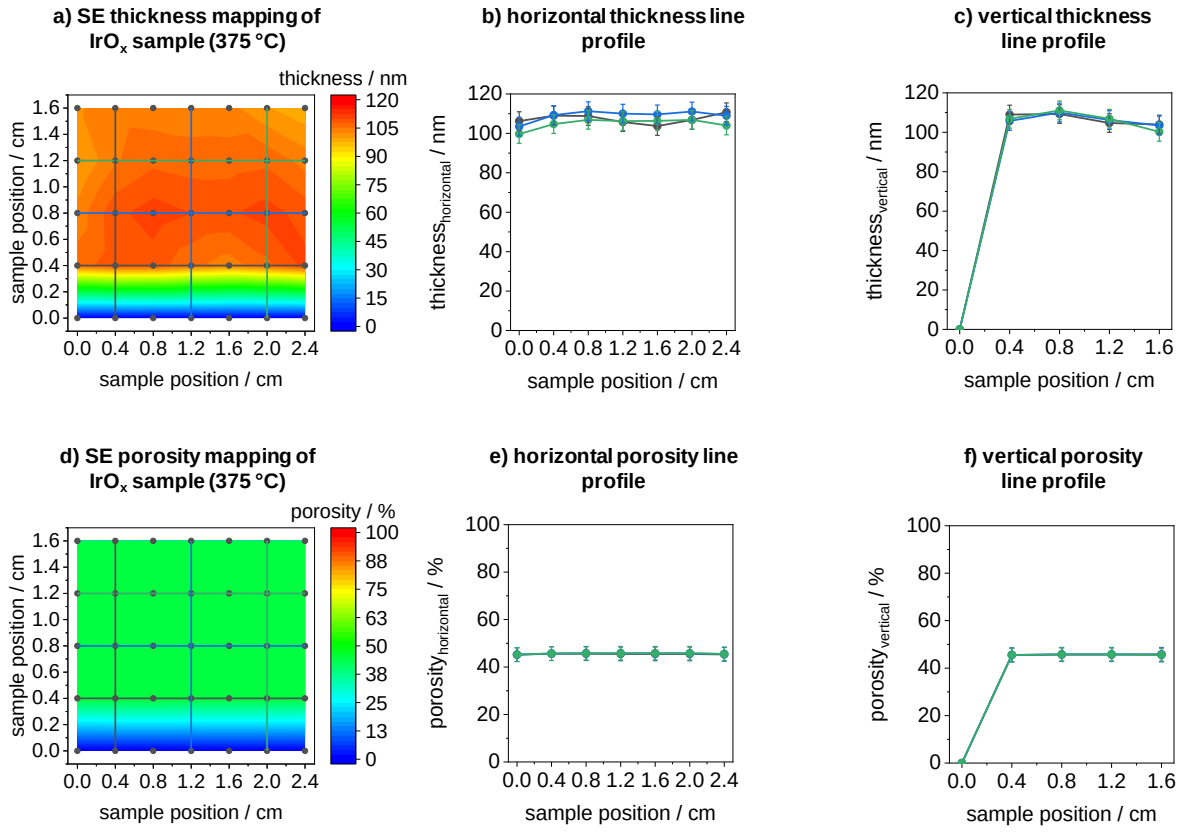

Figure S9: SE sample mapping of a mesoporous IrOx film on a Si wafer calcined at 375 °C in flowing air for 5 minutes. a) thickness mapping of the sample with indicated measuring points. b) horizontal and c) vertical thickness profiles of the sample. d) porosity mapping with line profiles in the horizontal (e) and vertical (f) direction.

SI 9. Ellipsometric porosimetry (EP) measurements of mesoporous iridium oxide films

Investigation of the change in the refractive index at a photon energy of 3 eV (413 nm) by varying the relative humidity between 0% and approx. 100%. The measurements were carried out in an environmental cell at a fixed angle of incidence (AOI) of 60°. The relative humidity was adjusted by mixing dry nitrogen gas with water-saturated nitrogen gas. The total N_2 flux was 2.5 L min^{-1}, controlled by two mass flow controllers and a constant temperature of 23 °C. The relative humidity was adjusted by mixing dry nitrogen gas with water-saturated nitrogen gas. The relative humidity was measured for the exiting gas and for each water partial pressure behind the cell. The model described in SI 5 was used for ellipsometric porosimetry measurements. Porosity, the pore geometry factor as well as the degree of pore filling with water served as free parameters.

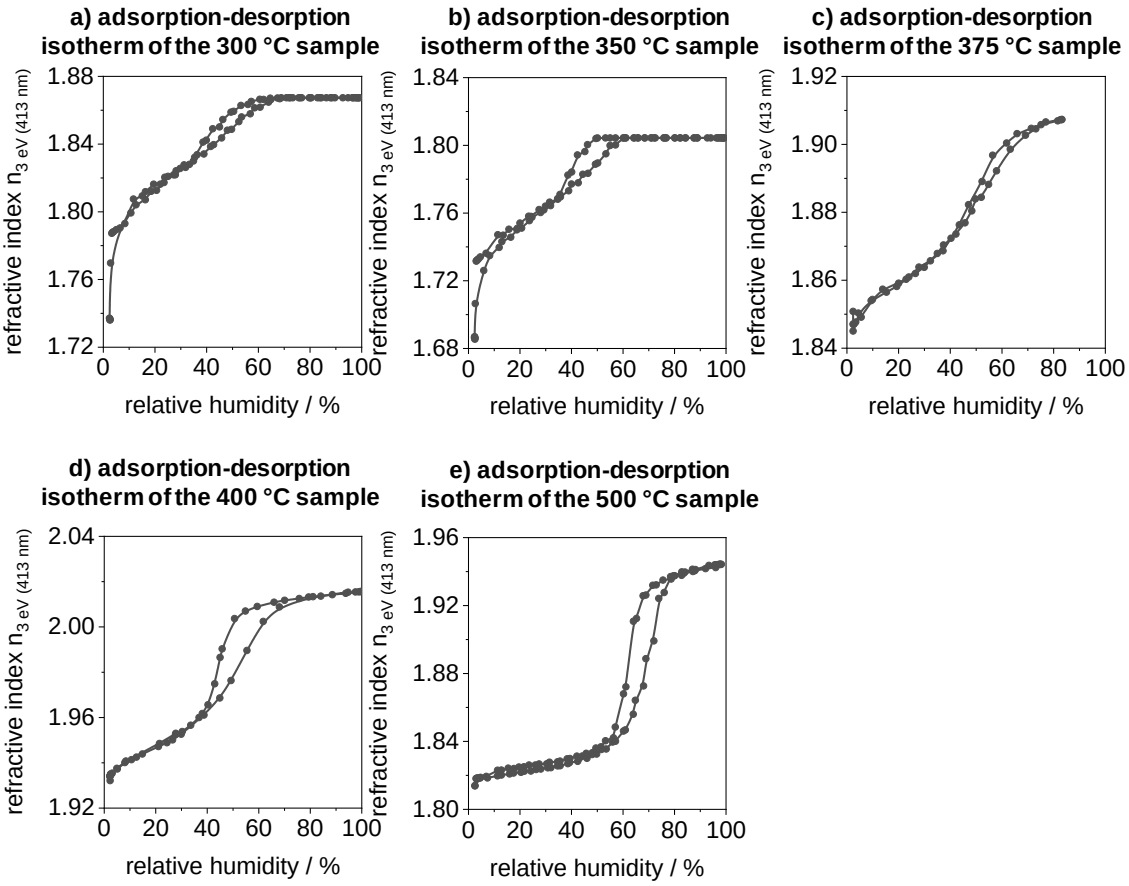

Figure S10: Adsorption-desorption isotherms, obtained from the change of the refractive index at a photon energy of 3 eV as a function of the relative humidity.

SI 10. Bulk electron energy loss spectra and correlation with intrinsic OER activities

Calculated bulk ELL spectra calculated from derived dielectric functions of iridium oxide films calcined between 300 °C and 600 °C. Figure S11a presents the bulk valence EEL spectra of the films with indication of two peaks (A_{bulk}, B_{bulk}). Figure S11b indicates the shift in the peak position of the A_{bulk} peak with increasing calcination temperature. Figure S11c displays the correlation between intrinsic OER activity and the peak position.

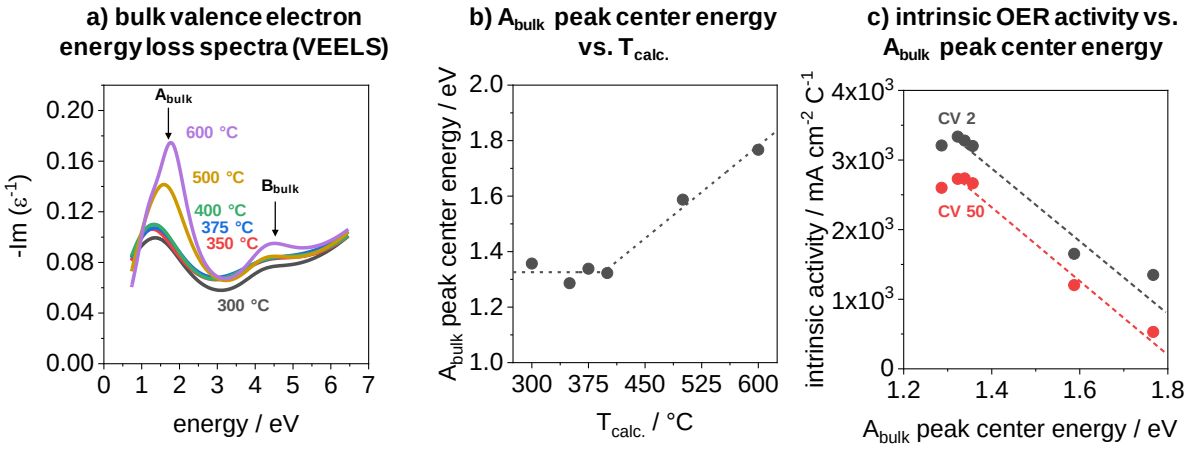

Figure S11: Bulk valence EEL spectra calculated from the dielectric functions of mesoporous iridium oxide films calcined between 300 °C and 600 °C. a) calculated bulk valence EEL spectra. b) center energy of the indicated A_{bulk} peak as a function of calcination temperature ($T_{calc.}$) and c) correlation between intrinsic OER activity and the shift of the A_{bulk} peak.

SI 11. Resonant photoemission spectroscopy (ResPES) and X-ray photoelectron spectroscopy (XPS)

The O K-edge were completed with ResPES collected in the valence band using excitation photon energies in the vicinity of the O 1s which are ascribed to an electronic transition from an occupied O 1s to an unoccupied O 2p hybridized with the Ir 5d orbitals. The valence band spectra have a satellite peak at around 15-25 eV. Going towards the O K-edge yields the formation of two main resonance peaks between 529-530 eV and between 531-534 eV. Beyond this excitation energy the off-resonance photoemission is recovered. The resonance peak around 529-530 eV is ascribed to the transition to the conduction band states formed by the hybridization of the O 2p–Ir 5d involving a coupling of O 2p with the t_{2g} at the unoccupied d_{xy}, d_{xz} and d_{yz} orbitals. Meanwhile the resonance peak around the 531-534 eV is ascribed to the hybridized O 2p with the e_g d_{x2-y2} and d_{z2} states. Increasing the calcination temperature from 300 to 600 °C has a significant influence on the resonance peak at around 529-530 eV due to the transition form mostly occupied t_{2g} orbitals in a μ_1-OH configuration (at low calcination temperatures) to an unoccupied μ_3-O configuration (at higher calcination temperatures) yielding the increase in the overall t_{2g} peak intensity. These measurements are in good agreement with the O K-edge spectra collected in TEY being ResPES measurements more surface sensitive.

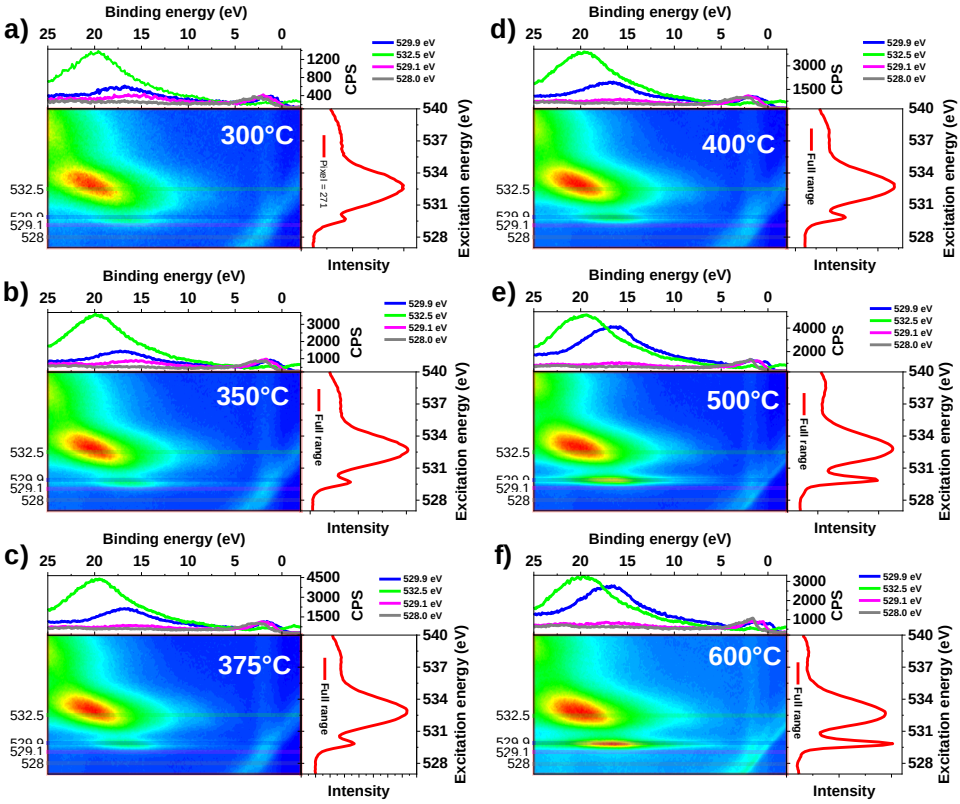

Figure S12: ResPES collected in the valence band using excitation photon energies in the vicinity of the O 1s for a) 300 °C, b) 350 °C, c) 375 °C, d) 400 °C, e) 500 °C and f) 600 °C calcination temperatures.

Figure S13 show the XPS measurements of IrO_x samples calcined between 300 and 600 °C. Figure S13a displays the survey measurement of the samples, Figure S13b the detailed spectra in the O 1s region and S10.2c the spectra in the Ir 4f region. The IrO_x film calcined at 300 °C shows a broad peak at around 531 eV in the O1s spectra, which can be attributed to a more hydrated oxygen species.[12] With increasing calcination temperature, the peak shifts to lower binding energies and corresponds to a more anhydrous oxygen species.[12] At 500 °C a shoulder become visible in the O 1s spectra which correspond to the oxidic Ir species. The Ir 4f spectra of the calcination series indicate a slight shift of the Ir $4f_{7/2}$ and $4f_{5/2}$ peak to lower binding energies with increasing temperature.[12]

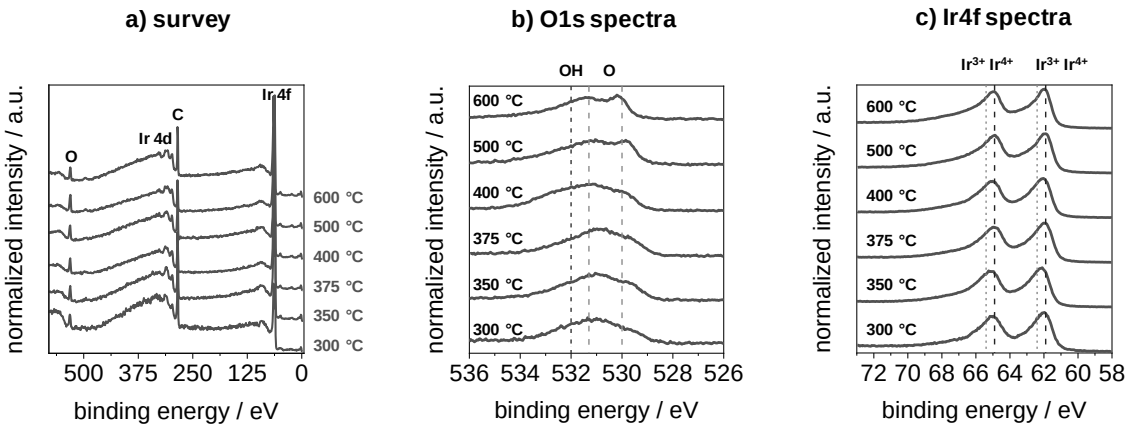

Figure S13: XPS measurements of the mesoporous IrO_x samples calcined between 300 and 600 °C in air. a) survey spectra of the different calcined samples, b) O1s spectra and c) spectra in the Ir4f region.

References

1. Wernecke, J.; Shard, A. G.; Krumrey, M., Traceable thickness determination of organic nanolayers by X-ray reflectometry. *Surface and Interface Analysis* **2014,** *46* (10-11), 911-914.

2. Gibaud, A.; Vignaud, G., Specular Reflectivity from Smooth and Rough Surfaces. In *X-ray and Neutron Reflectivity: Principles and Applications*, Daillant, J.; Gibaud, A., Eds. Springer Berlin Heidelberg: Berlin, Heidelberg, 2009; pp 85-131.

3. Henke, B. L.; Gullikson, E. M.; Davis, J. C., X-Ray Interactions: Photoabsorption, Scattering, Transmission, and Reflection at E = 50-30,000 eV, Z = 1-92. *Atomic Data and Nuclear Data Tables* **1993,** *54* (2), 181-342.

4. Goodman, J.; Weare, J., Ensemble samplers with affine invariance. *Comm. App. Math. and Comp. Sci.* **2010,** *5* (1), 65-80.

5. Foreman-Mackey, D.; Hogg, D. W.; Lang, D.; Goodman, J., emcee: The MCMC Hammer. *Publications of the Astronomical Society of the Pacific* **2013,** *125* (925), 306-312.

6. Hilfiker, J. N.; Singh, N.; Tiwald, T.; Convey, D.; Smith, S. M.; Baker, J. H.; Tompkins, H. G., Survey of methods to characterize thin absorbing films with Spectroscopic Ellipsometry. *Thin Solid Films* **2008,** *516* (22), 7979-7989.

7. Schmidt, D.; Schubert, M., Anisotropic Bruggeman effective medium approaches for slanted columnar thin films. *J. Appl. Phys.* **2013,** *114* (8), 083510.

8. Fujiwara, H., *Spectroscopic ellipsometry: principles and applications*. John Wiley & Sons: 2007; p 1-369.

9. Tompkins, H.; Irene, E. A., *Handbook of Ellipsometry*. William Andrew Publishing: 2005; p 1-891.

10. Tiwald, T. E.; Thompson, D. W.; Woollam, J. A.; Paulson, W.; Hance, R., Application of IR variable angle spectroscopic ellipsometry to the determination of free carrier concentration depth profiles. *Thin Solid Films* **1998,** *313-314*, 661-666.

11. Wooten, F., Chapter 3 - ABSORPTION AND DISPERSION. In *Optical Properties of Solids*, Wooten, F., Ed. Academic Press: 1972; pp 42-84.

12. Freakley, S. J.; Ruiz-Esquius, J.; Morgan, D. J., The X-ray photoelectron spectra of Ir, IrO_2 and $IrCl_3$ revisited. *Surface and Interface Analysis* **2017,** *49* (8), 794-799.